

CONDUCTION IN  $Y_{1-x}Sc_xBa_2Cu_3O_y$ A. Ulug<sup>a</sup>, B. Ulug<sup>a</sup>, H. I. Adiguzel<sup>1,b</sup><sup>a</sup>Akdeniz University, Faculty of Arts & Science, Dept. of Physics, Antalya, Turkey<sup>b</sup>Inönü University, Faculty of Arts & Science, Dept. of Physics, Malatya, Turkey

Received 1 October 2003, accepted 14 December 2004

Electrical conduction in  $Y_{1-x}Sc_xBa_2Cu_3O_y$  prepared in the range of  $x = 0.0 - 1.0$  was investigated. X-ray, infrared spectroscopy and electron microscope inspections were employed to develop an understanding for the structural properties of the samples. The results indicate that all the samples were multiphase even at  $x = 0.1$  due to probably the low solubility of Sc in  $YBa_2Cu_3O_y$ . The samples were found to be the mixtures of semiconductive and superconductive phases, the ratio of which determines the critical temperature,  $T_c$ , the resistance and temperature dependence of the resistance.  $T_c$  varied within a narrow range of 10 K until the semiconductivity appears at  $x = 0.9$ . It was argued that the  $Y_{1-x}Sc_xBa_2Cu_3O_y$  samples show semiconducting transition at a Sc content higher than the percolation threshold. Hopping mechanisms were found to be responsible for the conduction in  $Y_{0.1}Sc_{0.9}Ba_2Cu_3O_y$  in which the density of states at the Fermi level was obtained as  $6.0 \times 10^{21} \text{ m}^{-3} \text{ eV}^{-1}$ .

PACS: 74.72.Bk

## 1 Introduction

Element substitution has great importance in determining the mechanisms of high-temperature superconductivity. Many efforts have been made on different types of superconductors and remarkable progress has been achieved [1-3].

The substitution of Sc in  $YBa_2Cu_3O_y$  is attractive from a few points of view. At first,  $Sc^{3+}$  (ionic radius  $r = 0.073 \text{ nm}$ ) is a lighter and smaller alternative of isovalent  $Y^{3+}$  ( $r = 0.089 \text{ nm}$ ) and  $La^{3+}$  ( $r = 0.102 \text{ nm}$ ). If  $Sc^{3+}$  is substituted to Y site, the conduction in CuO layers can be influenced without altering the charge balance of the structure; small  $Sc^{3+}$  ion in  $Y^{3+}$  site might cause CuO planes to approach each other. As a consequence, some increases in the buckling angle of CuO planes and in the internal stresses are expected. On the other hand,  $Sc^{3+}$  having almost the same ionic radius with  $Cu^{2+}$  ( $r = 0.072 \text{ nm}$ ) might go into the square pyramidal oxygen environment of the perovskite structure and replaces some Cu ions. In this case the ratio of  $Cu^{3+}/Cu^{2+}$ , and thus the superconductivity might be altered [4]. More interesting is the magnetic behaviour; a paramagnetic spin equivalent of  $2.7\mu_B$  per Sc ion which is the same as  $Y^{3+}$  and  $La^{3+}$  but different from  $Cu^{2+}$  was deduced from the Curie susceptibility [5]. Therefore,

<sup>1</sup>E-mail address: iadiguzel@inonu.edu.tr

if Sc is substituted to Cu sites the magnetic structure of the unit cell as well as the stoichiometry of CuO layers can also be altered.

In this work, the electrical conduction in the normal state of  $Y_{1-x}Sc_xBa_2Cu_3O_y$  ceramic compounds is discussed in the light of the new electrical and the structural data obtained.

## 2 Experiment

Samples were prepared from high-purity (99.9 %) powders of  $Sc_2O_3$ ,  $Y_2O_3$ ,  $BaCO_3$ , and  $CuO$ . The nominal compositions of  $Y_{1-x}Sc_xBa_2Cu_3O_y$  were prepared in the range of  $x = 0.0 - 1.0$  with an increment of 0.1. The powders were calcinated in flowing oxygen at  $900^\circ C$  for 16 h. After pelletising, the samples were sintered for 16 h in flowing oxygen at  $950^\circ C$ . Pelletising and sintering procedure was repeated three times. In order to assure the maximum oxygen intake, the samples were slowly cooled down to room temperature at a rate of 1 K/min in flowing oxygen during the last annealing cycles.  $ScBaCuO_y$  reference samples were also synthesized as described in Ref. 6.

Conductivity of low-resistance samples was measured by the standard fourprobe technique. The temperature of the samples was kept at a predefined one by a closed cycle refrigeration system, Leybold R210, equipped with a calibrated Si diode and a temperature controller, LakeShore DRC-91CA. The actual sample temperature was calculated by averaging the temperature readings taken just before and after the resistance readings around each predefined temperature. A constant current of 1 mA was passed through the samples and the voltage drop across the voltage leads was read by a Keithley 182 nanovoltmeter. Another voltage reading was accomplished immediately after reversing the current polarity. This procedure was repeated 10 times, and the average of twenty readings was then taken as the resistance value at the average sample temperature.

X-ray studies were carried out on a powder diffractometer, Rigaku-RadB, at room temperature. A JEOL JXA-840 system was employed for the energy dispersive analysis of x-ray (EDAX) and scanning electron microscope (SEM) inspections. Infrared (IR) absorbance spectra of the samples were obtained in the frequency range of  $40-80\text{ mm}^{-1}$  with a resolution of  $0.1\text{ mm}^{-1}$  at room temperature using a Fourier Transform Infrared (FTIR) spectrophotometer, Bomem MB-100. Preheated KBr powder was employed as a reference material.

## 3 Results and Discussion

The x-ray diffractions (XRD) of  $Y_{1-x}Sc_xBa_2Cu_3O_y$  are given in Fig. 1. The sample with  $x = 0$  reveals almost a single phase  $YBa_2Cu_3O_y$  as shown in Fig. 1, in which all the peaks are indexed on the basis of Pmmm symmetry and orthorhombic unit cell with the lattice parameters of  $a = 0.3822 \pm 0.0001\text{ nm}$ ,  $b = 0.3893 \pm 0.0001$ , and  $c = 1.1682 \pm 0.0002\text{ nm}$ . The peaks observed at  $x = 0.0$  appear even for  $x = 1.0$  though they get considerably weak. Among the others, the peaks emerging at the diffraction angles ( $2\theta$ )  $28.35$ ,  $29.25$ ,  $30.00$ ,  $33.90$ ,  $49.20^\circ$ , and  $29.72$ ,  $32.50$ ,  $42.78$ ,  $53.06^\circ$  are associated with  $BaCuO_2$  and  $ScBaCuO_y$ , respectively. The small peaks emerging at  $2\theta = 29.86^\circ$  and  $30.55^\circ$  are interpreted as due to  $Y_2BaCuO_5$  and only the peak observed at  $2\theta = 35.50^\circ$  is matched with the ones of  $CuO$ . XRD in Fig. 1 indicates that  $ScBa_2Cu_3O_y$  has perovskite structure whereas  $ScBaCuO_y$  that exists even at  $x = 0.1$  in the

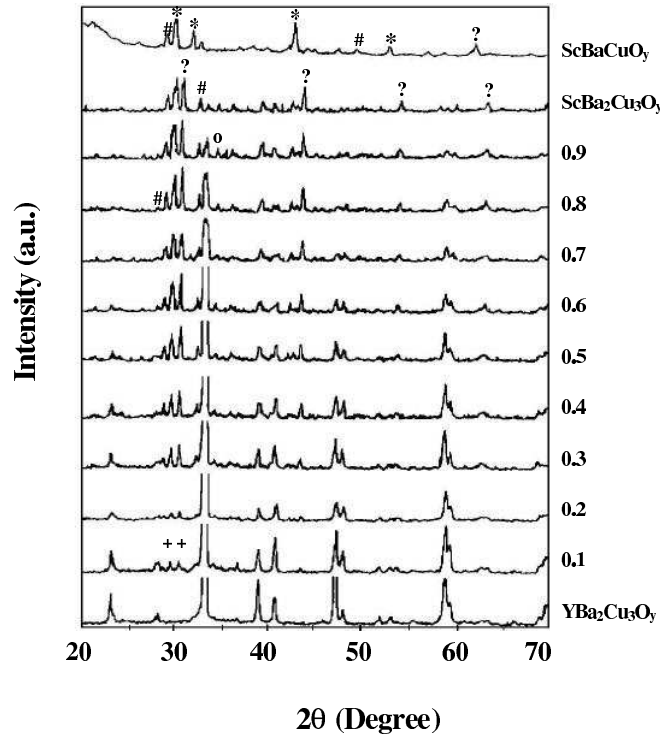


Fig. 1. X-ray powder diffractograms of  $ScBaCuO_y$  and  $Y_{1-x}Sc_xBa_2Cu_3O_y$  for  $0.0 \leq x \leq 1.0$ . Numbers near the plots indicate the Sc content of the samples.  $\square$  –  $YBa_2Cu_3O_y$ ,  $+$  –  $Y_2BaCuO_5$ ,  $\#$  –  $BaCuO_2$ ,  $*$  –  $ScBaCuO_y$ ,  $o$  –  $CuO$ ,  $?$  – Unknown.

samples has quite a different structure from the perovskites. No appreciable shift in the position of XRD peaks are observed with  $x$ . Although such shifts are expected for the substitution of Cu sites by Sc but they would be surprising for the Y site substitution.

IR absorbance spectra of the samples given in Fig. 2 show that the peaks not belonging to  $YBa_2Cu_3O_y$  emerge at  $x = 0.1$  and grow monotonously with  $x$ . This is consistent with the result reached so far by the XRD analysis. The IR absorbance spectra of  $ScBaCuO_y$  and  $Y_{1-x}Sc_xBa_2Cu_3O_y$  in Fig. 2 clearly show that the strong peaks around 48.0, 52.5, 54.0, and 65.5  $mm^{-1}$  are basically originate from  $ScBaCuO_y$ , though  $CuO$ ,  $BaCuO_2$ , and  $Y_2BaCuO_5$  having peaks at 47.6/52.5, 47.7/52.5, and 54.0  $mm^{-1}$ , respectively, might also have some contribution [7,8].  $CuO$  and  $BaCuO_2$  revealing peaks at 44.7 and 45.4  $mm^{-1}$ , respectively, are also thought responsible for the shoulder between 44.0 and 45.0  $mm^{-1}$ . Despite the fact that  $Y_2BaCuO_5$  and  $CuO$  reveal peaks at 41.65 and 42.1  $mm^{-1}$ , respectively, the bump at 41.8  $mm^{-1}$  is believed to originate from Cu-O vibration modes in perovskite structure since it appears for all  $x$ , including  $YBa_2Cu_3O_y$  and  $ScBa_2Cu_3O_y$ , but  $ScBaCuO_y$ . Above argument for the small peak at 42.0  $mm^{-1}$  could also be carried for the shoulder at 38.0  $mm^{-1}$  since they exhibit similar properties. As far as the strong peak around 40.0  $mm^{-1}$  is concerned some care is required, because,

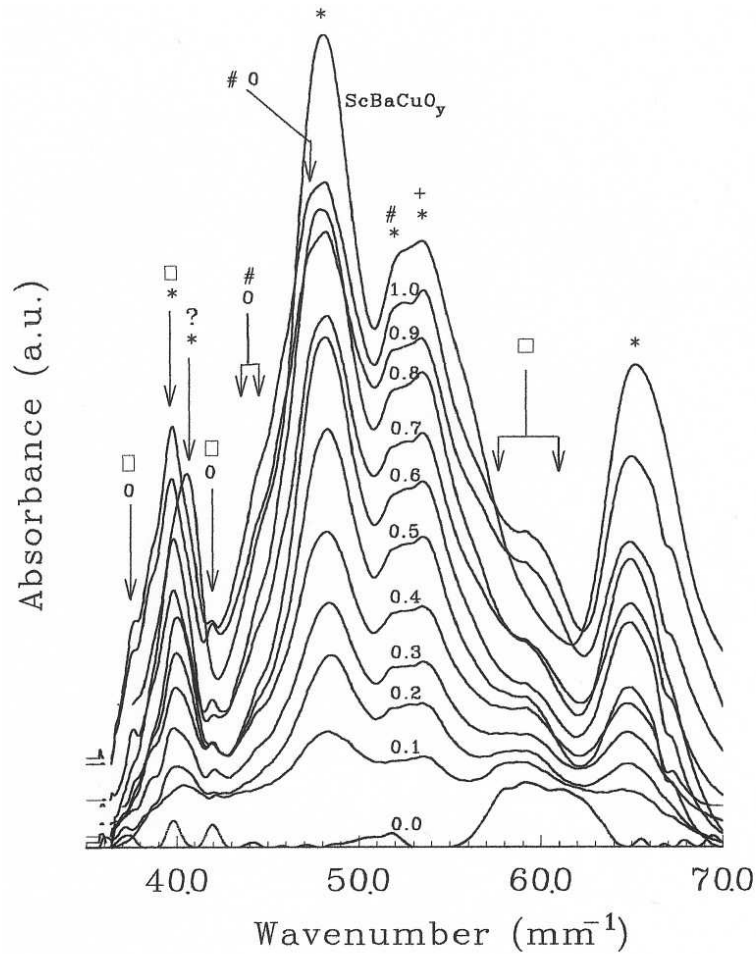


Fig. 2. IR absorption spectra of  $\text{ScBaCuO}_y$  and  $\text{Y}_{1-x}\text{Sc}_x\text{Ba}_2\text{Cu}_3\text{O}_y$  for  $0.0 \leq x \leq 1.0$ . Decimal numbers indicate the Sc content of the samples. The spectra are shifted upward in absorbance scale for clarity. □ –  $\text{YBa}_2\text{Cu}_3\text{O}_y$ , + –  $\text{Y}_2\text{BaCuO}_5$ , # –  $\text{BaCuO}_2$ , o –  $\text{CuO}$ , \* –  $\text{ScBaCuO}_y$ , ? – Unknown.

$\text{YBa}_2\text{Cu}_3\text{O}_y$  and  $\text{ScBa}_2\text{Cu}_3\text{O}_y$  both reveal peaks at  $39.8 \text{ mm}^{-1}$  while  $\text{ScBaCuO}_y$  has a peak at  $40.8 \text{ mm}^{-1}$ . As XRD results indicate, Sc inclusion stimulates the formation of  $\text{ScBaCuO}_y$  and  $\text{ScBa}_2\text{Cu}_3\text{O}_y$  while reducing the  $\text{YBa}_2\text{Cu}_3\text{O}_y$  concentration in the samples. Thus, the shape and the position of the peak about  $40.0 \text{ mm}^{-1}$  are defined by the ratio of  $\text{ScBaCuO}_y$  in the samples.

The broad band emerging between  $57.0$  and  $64.0 \text{ mm}^{-1}$  in Fig. 2 are due to  $\text{YBa}_2\text{Cu}_3\text{O}_y$ ; the one appearing at  $57.3 \text{ mm}^{-1}$  is attributed to the axial antisymmetric stretching mode while the one at  $62.0 \text{ mm}^{-1}$  has been attributed to the  $\text{Cu}(1)\text{--O}(4)$  vibrations [9]. These modes are sensitive to the oxygen content and shift from  $57.3 \text{ mm}^{-1}$  to  $59.1 \text{ mm}^{-1}$  and from  $62.5 \text{ mm}^{-1}$  to  $64.7 \text{ mm}^{-1}$ , respectively, as the oxygen content approaches to 7 [10]. The existence of these

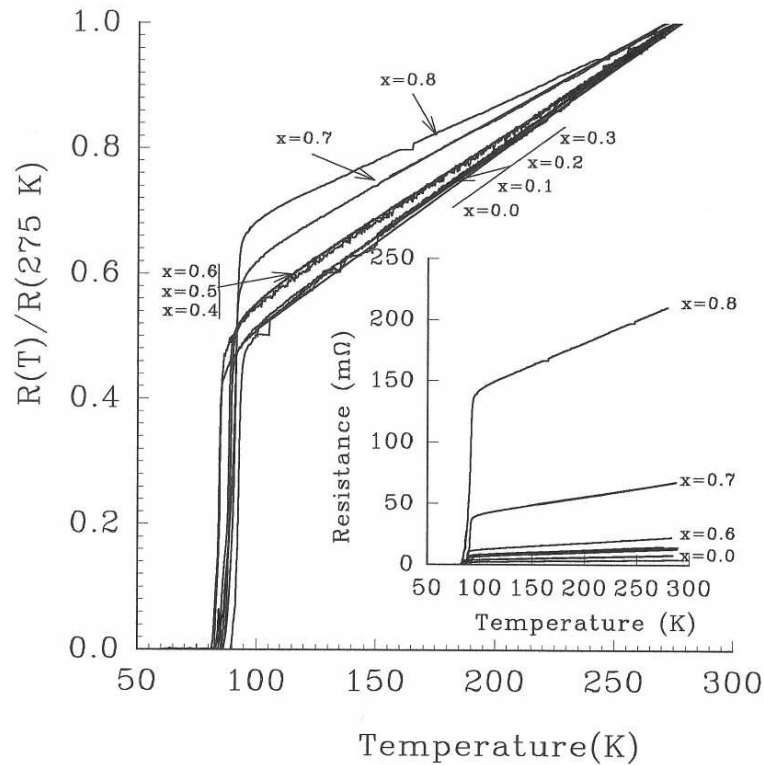


Fig. 3. Temperature dependence of the normalized resistance of  $Y_{1-x}Sc_xBa_2Cu_3O_y$  for  $x \leq 0.8$ . Inset shows the change in absolute resistance values.

phonon modes in IR spectra of the samples indicates that  $YBa_2Cu_3O_y$  phonon modes exist for  $x \leq 1.0$  and supports the XRD result that  $ScBa_2Cu_3O_y$  might have perovskite structure. IR spectra also confirm the XRD results that the samples consist of  $YBa_2Cu_3O_y$  and some other phases (mainly  $ScBa_2Cu_3O_y$ ,  $ScBaCuO_y$ ,  $BaCuO_2$  etc.) that remain same throughout the whole compositional range. In fact, EDAX inspections indicate that besides  $YBa_2Cu_3O_y$ , the samples contain  $Y_2BaCuO_5$ ,  $Ba_2CuO_y$ ,  $BaCuO_2$ ,  $ScBaCuO_{3.5}$ ,  $CuO$ , and  $Cu_{1.85}Y_{0.9}$  for up to  $x = 0.9$ . Intense peaks between  $50.0$  and  $70.0 \text{ mm}^{-1}$  make impossible to comment on the buckling angle of  $CuO$  planes whose vibration modes are expected in this range.

The resistance values of the samples are normalised by their values at 275 K are shown in Fig. 3 while the inset shows the absolute resistance values for the same temperature range. Contrary to the data reported in the literature that showed semiconductivity for  $x \geq 0.325$  [11] and  $x \geq 0.7$  [12] our samples exhibited superconductivity for up to  $x = 0.8$ . The data presented in Fig. 3 reveal that increase in Sc content does not influence the temperature slope and  $T_c$  much, though the resistance values are affected drastically: For  $x \leq 0.6$ , the samples display good metallic behaviour with about the same temperature slope as  $YBa_2Cu_3O_y$  demonstrates. Samples with  $x = 0.7$  and  $x = 0.8$  reveal slightly smaller temperature slopes than the others in

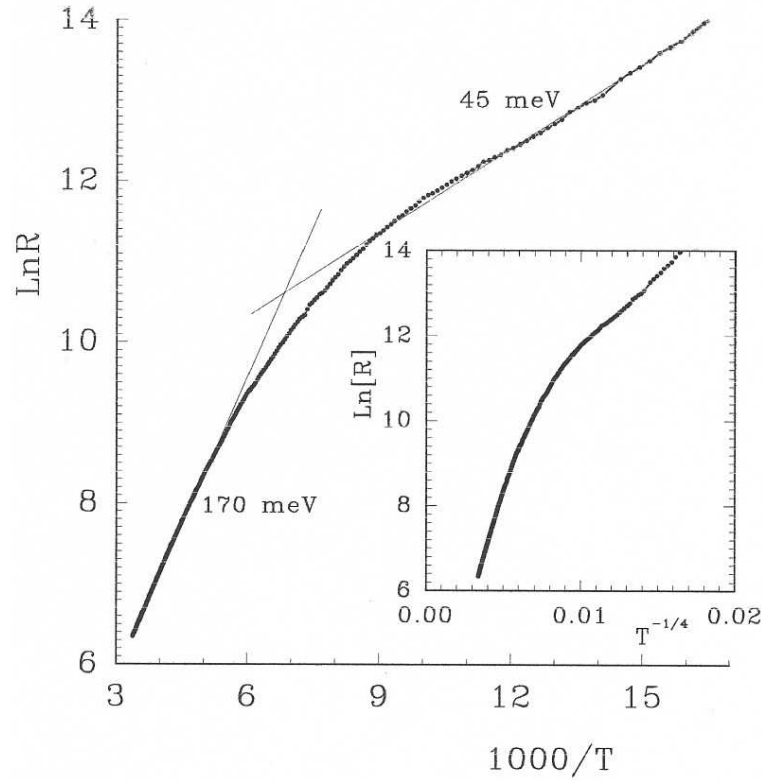


Fig. 4. Arhenius plot for  $Y_{0.1}Sc_{0.9}Ba_2Cu_3O_y$ . Activation energies calculated from the corresponding slopes are also given. Inset shows  $\ln[R]$  vs.  $T^{-1/4}$  plot.

the normal state while they possess high resistance values. It should be noted that  $T_c$  varies in a narrow range of 10 K for  $0.0 \leq x \leq 0.8$ . The temperature slope and the resistance values of the samples exhibit abrupt change between  $x = 0.8$  and  $x = 0.9$ , Fig. 3 and Fig. 4.

The possibility of Sc substitution in Cu sites could be excluded since the data presented in Fig. 3 reveal that the temperature slope in the normal state is not affected much from the Sc inclusion for  $x < 0.9$ : Cu site inclusions in  $YBa_2Cu_3O_y$  systems are known to influence the temperature slope drastically even at low concentrations [12]. As discussed above, XRD and FTIR data indicate that the solubility of Sc in  $YBa_2Cu_3O_y$  is rather low and Sc somehow promotes the formation of semiconducting phases, Fig. 4. Our samples, in fact, appear as the mixtures of superconductive and semiconductive phases in which the ratio of the semiconductive phase increases with Sc.

In such a medium, current flows through low resistance paths consisting of superconducting  $YBa_2Cu_3O_y$  grains [13]. Electron scattering at the grain boundaries and within the grains along the backbone would therefore define  $T_c$ , the resistance value and the temperature dependence of the samples. In this scenario,  $T_c$  and the resistance values are expected to remain same as in  $YBa_2Cu_3O_y$  until the superconducting backbone is broken.

The semiconductivity first appears between  $x > 0.8$  and  $x \leq 0.9$ , Fig. 3 and Fig. 4. The percolation threshold,  $p_c$ , at which a conducting path between two opposite electrodes is established for the first time in a conducting/non-conducting mixture varies between 0.47 and 0.15 for two- and three-dimensional systems, respectively [14]. If the superconducting path is assumed to break at  $1-x$ , thus, the Sc concentration at which the superconducting/semiconducting transition takes place is in good agreement with the percolation prediction. The Sc content at which a jump in resistance is first observed,  $0.6 < x \leq 0.7$  in Fig. 3, however, needs to be explained. It should also be noted that  $T_c$  and the linearity of the normal state are not influenced much with Sc inclusion, Fig. 3. Such properties are not specific to  $Y_{1-x}Sc_xBa_2Cu_3O_y$  alone but seem to be common for some ceramic superconductors, e.g.,  $Y_{1-x}Ca_xBa_2Cu_3O_y$  [15] and  $YBa_{2-x}Sr_xBa_2Cu_3O_y$  [16].

The scattering of the charge carriers at the grain boundaries would be responsible for the above properties. Scattering at the grain boundaries would be expected to deteriorate as the Sc content increases since increase in  $x$  stimulates the formation of semiconducting phases. Furthermore, the current would flow through the longer paths since the short paths would no longer be available to charge carriers as the percolation threshold is approached [17,18]. Thus, the number of grain boundaries and the resistance along the long current paths would be increased though the temperature dependence of the conduction remains same due to the fact that the scattering of the charge carriers at the grain boundary is not a temperature dependent mechanism.

The scattering at the grain boundaries can be assumed to destroy the superconductivity after the length of deterioration becomes compatible with the coherence length of the carriers, which should be more than the extend of the states in the semiconducting phase at a composition where the semiconductivity first appear. The extent of the states can be obtained if the temperatures above 150 K are assumed to be the region of freezing out of the carriers in Fig. 4 [19]. Under the assumptions that the magnitude of the activation energy is close to the ionisation energy of an isolated state and the effective mass of the electrons is equal to the effective mass of a free electron, the radius of the state is calculated as 0.68 nm for the temperatures above 150 K. The magnitude of the radius of the states, which is approximately  $1.78a$ , indicates that the superconductivity would be retained for some  $x$  after the superconducting paths are broken at the percolation threshold.

Arrhenius plot given in Fig. 4 for  $Y_{0.1}Sc_{0.9}Ba_2Cu_3O_y$  shows two distinct linear regions whose activation energies decrease from 170 meV to 45 meV as the temperature is lowered. Decrease in activation energy and the linear properties displayed in  $\ln R$  vs.  $T^{-1/4}$  plot, inset in Fig. 4, at low temperatures suggest the hopping mechanisms. The density of states at the Fermi level,  $N(E_F)$ , is evaluated as  $6.0 \times 10^{21} \text{ m}^{-3} \text{ eV}^{-1}$  from the low temperature slope of  $\ln[R/T^{1/2}]$  vs.  $T^{-1/4}$  plot by taking the spatial extent of the localized states as the radius of the localized states calculated above (i.e., 0.68 nm). The  $N(E_F)$  and the most probable hopping distance obtained ( $\approx 13T^{-1/4}$ , e.g., 3.75 nm at 150 K) are comparable with the value commonly encountered in doped semiconductors [19].

#### 4 Conclusion

The results obtained in this work confirm the earlier reports that the solubility of Sc is rather low in  $YBa_2Cu_3O_y$ . So, the samples appear as a multiphase system even at the low Sc content; the samples are the mixtures of superconducting  $YBa_2Cu_3O_y$  and some semiconducting phases

whose ratio altered with the Sc content. The resistance data indicate that the current flows along the low resistance paths in the samples. It was argued that  $Y_{1-x}Sc_xBa_2Cu_3O_y$  samples show semiconducting transition above the Sc content at which the superconducting current paths are broken at the percolation threshold. Hopping mechanisms seem responsible for the electrical conduction in semiconducting  $Y_{0.1}Sc_{0.9}Ba_2Cu_3O_y$ .

**Acknowledgement:** This project is supported by the Akdeniz University Research Fund (Project No: AÜAF. 98.01.0105.02)

### References

- [1] X. Z. Wang, B. Helebrand, D. Bauerle: *Physica C* **200** (1992) 12
- [2] S. I. Yoo, N. Sakai, H. Takaichi, T. Higuchi, M. Murakami: *Appl. Phys. Lett.* **65** (1994) 633
- [3] L. Gao, Y. Y. Xue, F. Chen, Q. Xiong, R. L. Meng, D. Ramirez, C. W. Chu: *Phys. Rev. B* **50** (1997) 4260
- [4] B. R. Zao, Y. H. Shi, Y. Lu, H. S. Wang, Y. Y. Zao, L. Li: *Solid State Commun.* **63** (1987) 409
- [5] J. T. Markert, Y. Dalichaouch, M. B. Maple: *Physical Properties of high Temperature Superconductors I*. World Scientific, Singapore 1989
- [6] G. Svensson, Z. Hegedüs, L. Wang, Ö. Rapp: *Physica C* **153-155** (1988) 864
- [7] A. Ulug: *PhD Thesis*. İnönü University, Institute of Science, Turkey 1994
- [8] G. Ruani, C. Taliani, R. Zamboni, D. Cittone, F. C. Matarotta: *J. Optical Soc. Am. B – Optical Phys.* **6** (1989) 409
- [9] G. Burns, F. H. Dacol, P. Freitas, T. S. Plaskett, W. König: *Solid State Commun.* **65** (1987) 471
- [10] W. S. Zeng, Z. F. Li, G. Y. Zhang, S. L. Yan, G. C. Xiong, S. Z. Wang: *Infrared Phys.* **33** (1992) 459
- [11] Y. H. Shi, H. S. Weng, Y. G. Wang, Y. Lu, B. R. Zhao, Y. Y. Zhao, L. Li: *Solid State Commun.* **63** (1987) 641
- [12] N. Mori: *Jpn. J. of Appl. Phys.* **28** (1989) 980
- [13] K. V. Rao: *Rev. of Solid State Sci.* **1** (1987) 259
- [14] G. E. Pike, C. H. Seager: *Phys. Rev. B* **10** (1974) 1421
- [15] A. Ulug, B. Ulug: *Mater. Chem. and Phys.* **76** (2002) 299
- [16] A. Ulug, B. Ulug, E. Sener: *J. Appl. Phys.* **80** (1996) 2317
- [17] D. Stauffer: *Phys. Rep.* **54** (1979) 1
- [18] A. Aharony: *Europhys. News* **17** (1986) 41
- [19] B. I. Shklovski. A. A. Epros: *Electronic Properties of Doped Semiconductors*. Springer, Berlin 1984